Surface-induced assembly of sophorolipids

Jessie Peyre, Ahmed Hamraoui, Marco Faustini, Vincent Humblot, Niki Baccile

PAPER

Surface-induced assembly of sophorolipids†

Jessie Peyre,[a] Ahmed Hamraoui,[ab] Marco Faustini,[a] Vincent Humblot[c] and Niki Baccile*[a]

Cite this: DOI: 10.1039/c7cp01339f

Received 1st March 2017,
Accepted 3rd May 2017

DOI: 10.1039/c7cp01339f

The surface self-assembly properties of acidic sophorolipids, a bolaform microbial glycolipids with pH-responsive properties in solution, were studied based on the chemical nature of the support and pH of the solution. Sophorolipids generally form micelles in water but formation of morphologies like platelets and twisted fibers depending on pH have also been reported. The surface self-assembly was achieved using dip-coating on three different substrates namely gold, silicon(111) and TiO_2 anatase. Deposition conditions (dip-coating withdrawal speed, relative humidity, temperature) were tested, and it was found that optimum self-assembly occurred at a withdrawal speed of 1 mm s^{-1}, T of 25 °C and relative humidity of 25%. The local structure of the sophorolipid films was characterized by Atomic Force Microscopy, while Scanning Electron Microscopy was used to characterize the spatial homogeneity. We also attempted to correlate dispersive, electron donor and electron attractor surface energy components, using Good–Van Oss's approach, and the behavior of sophorolipids. We found that when the surface energy is dominated by dispersive components, sophorolipids spontaneously assemble into entangled needles at all pH values (4, 6 and 11). However, when the surface energy is dominated by electronic components, pH has a strong influence on the surface self-assembly. We could discriminate three major organizations: homogeneous layer, isolated aggregates and a two-dimensional network similar to block copolymer surface self-assembly.

Introduction

Surface patterning has been applied extensively in material sciences fields like superhydrophobicity,[1] understanding wetting and dewetting phenomena,[2] conceiving lab-on-a-chip materials for biology and medicine,[3,4] and engineering surfaces with optimal physical properties such as semi-conduction,[5] light emission[6] or quantum barrier[7] or the enhancement of Raman spectroscopy.[8] There are two main approaches to obtain patterned surfaces: top-down and bottom-up methods.[9] The top-down techniques refer to physical or combined physical-chemical modification of a surface; well-known examples are photolithography,[10,11] soft lithography,[12–14] electron beam lithography[15] or etching.[16] The bottom-up approach, more recent in time and involving self-assembly, dewetting or a combination of both, has been widely explored due to its low cost and no involvement of large-scale apparatus. Block copolymers have been intensively explored as they are known to assemble spontaneously on planar surfaces or when constrained as thin films.[17–20] Modification of hydrophobic/hydrophilic block ratio,[21] or the chemical nature of one block,[22] are well-known methods to change the wettability of a surface and influence the surface pattern. Even though these approaches are well-established, drawbacks exist in terms of tedious process involved in controlling homogeneity[23] and the necessity of solvent and temperature annealing.[24–27] Although it is difficult to control large-scale and local order simultaneously,[23] considerable studies are available on multi-scale patterning achieving both chemical affinity between copolymers and controlling the evaporative self-assembly.[28]

The phase diagram of ionic surfactants is less rich compared to that of block copolymers, and they are less resistant to rinsing. They are an interesting alternative as their liquid–solid

[a] Sorbonne Universités, UPMC Univ Paris 06, CNRS, Collège de France UMR 7574, Chimie de la Matière Condensée de Paris, UMR 7574, F-75005 Paris, France. E-mail: niki.baccile@upmc.fr
[b] Université Paris Descartes, Faculté des Sciences Fondamentales et Biomédicales, 45 rue des Saints-Pères, 75006 Paris, France
[c] Sorbonne Universités, UPMC Univ Paris 06, CNRS, Laboratoire de Réactivité de Surface, UMR 7197, 4 Place Jussieu, 75005 Paris, France

† Electronic supplementary information (ESI) available: Scheme of the area was scanned by AFM and SEM techniques. AFM images of the control silicon, TiO_2 and gold surfaces, SEM images for dip-coated solutions of sophorolipids and two reference molecules (SDS and APG) at different pH, dip-coated solutions of sophorolipids at different temperatures and different humidity rate on silicon samples were obtained. SEM images were registered for dip-coated solutions of sophorolipids at different pH on gold and titanium dioxide samples; AFM images of surface self-assembly of the sophorolipids onto silicon at different temperatures were also obtained. The area of aggregates was observed at pH 6; values of contact angles were measured for each surface with milli-Q water, diiodomethane, formamide and glycerol and the values of surface tension components were relative to each solvent. See DOI: 10.1039/c7cp01339f

interfacial properties like fingering instabilities have been known since decades. The fingering instabilities originate from the presence of surface tension gradients across a thin liquid film of uniform height, which induces shear stress at air–liquid interface and drives the liquid from areas of low surface tension to areas of high surface tension. This results in height variations of the interface: the Marangoni flow.[29,30] In particular, the impact of spontaneous self-assembled monolayer formation on macroscopic phenomena like dewetting, driven by autophobing effect is of great interest.[31] The latter happens when a cationic surfactant is attracted by a negatively charged surface, thereby, exposing the hydrocarbon tail outwards, an event which induces a local increase in the contact angle and consequently poor wettability.[32–35] Dewetting of surfactant solutions originate from this effect, although other mechanisms and more complex local phenomena involving aqueous film thinning due to local inward or lateral water flows have been described.[36] Insights into the dewetting phenomena in surfactant solutions can be of major interest to control surface structures at different scales, as shown by Zelcer *et al.* in the formation of meso-macroporous silica thin films.[37] In a recent study, we showed the possibility of using microbial sophorolipid biosurfactants to prepare meso-macroporous silica thin films, where the macroporosity was probably due to a dewetting phenomenon caused by the presence of a sophorolipid.[38] Due to poor control of the dewetting phenomena, the behaviour of a sophorolipid at the liquid–solid interface had to be studied in detail.

In this study, we wanted to explore surface-patterning effects of a functional lipid amphiphile bearing pH-responsive carboxylic acid group and show that surface patterning can be induced by both pH and chemical nature of the surface. Small lipids have the advantage of rapid self-assembly without the requirement of additional annealing processes. We have shown in the present investigation that surface patterning can be obtained in water using dip-coating as a simple and fast deposition technique as it allows to control the physicochemical parameters such as temperature and relative humidity, compared to spin-coating. The experiments have been performed using sophorolipids,[39,40] a class of microbial glycolipids obtained from yeasts.[41–45] They have been studied for the last 20 years because of their low carbon footprint and their extensive applications as antibacterial and antifungal agents,[46,47] activity against cancer cells,[48,49] cosmetic products[50,51] and biosurfactants.[52–54] The solution properties of non-acetylated, monounsaturated, acidic sophorolipids (SL, see Fig. 1), and in particular their pH-responsive self-assembly have been shown earlier.[55–57] It has also been established that the structure of the molecules greatly influenced the self-assembly.[58] Acidic monounsaturated sophorolipids form ellipsoidal micelles in water in a very broad pH range (from pH 11 to pH 3),[59] although at basic pH, formation of nanoplatelets is also observed.[60] We also reported the micellar structure and their surface charge induced by pH.[61,62] The same molecules were also reported to form giant ribbons.[55,58] We have recently shown that the micelle-ribbon duality depends on purity; a standard non-acetylated, monounsaturated, acidic sophorolipid batch forms micelles, unless it is contaminated with 15 wt% of the saturated congener, which induces the ribbon formation.[63] In terms of surface-adsorption properties of the sophorolipids, only alkyl ester derivatives have been explored, which nonetheless have shown adsorption on alumina being two orders of magnitude higher than on silica beyond a solution concentration of 10^{-4} M.[64]

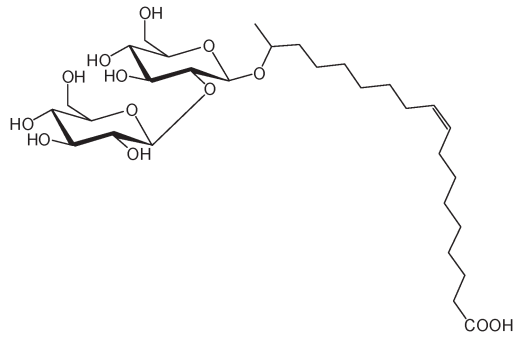

Fig. 1 Non-acetylated, monounsaturated, acidic form of C18:1 sophorolipid.

The surface self-assembly and patterning ability of an aqueous micellar solution of non-acetylated, monounsaturated, acidic sophorolipids have been shown in the present investigation. We have investigated both the pH influence and the crucial role of the underlying surface (silica, gold, titanium dioxide-anatase structure). Moreover, to the best of our knowledge, a connection between the behaviour of the sophorolipid solution and the surface energies of the selected materials has been established. To the best our knowledge, this link has not been proposed in earlier studies investigating the liquid–solid properties of surfactant solutions.

Experimental

Materials

Silicon wafers (polished) were purchased from MEMC Ipoh and gold wafers were purchased from Arrandee (Werther, Germany). Sophorolipids have been purchased from Soliance (France) and hydrolyzed in alkaline medium. pH was lowered to about 4.5 to obtain an open acidic form. They have been recovered using method 1 as reported in a previous study by Baccile *et al.*[65] Their purity has been evaluated at about 90% of both terminal and subterminal C18:1 congener and their equilibrium state in water is micellar as described earlier.[56,62,66] Sodium dodecyl sulfate (SDS) has been purchased from Aldrich and used as received. C10-Alkylpolyglycoside (APG, commercial name: Oramix) was provided by SEPPIC (France). All the solvents obtained from Sigma-Aldrich were used as received.

Preparation of samples

Silicon(111) wafers. The wafers were cut using a diamond pen, washed with absolute ethanol and then air dried just before dip-coating.

Titanium oxide (anatase) samples. The synthesis of the TiO_2 anatase thin film has been adapted from a previous study;

however, the addition of a porogen was excluded.[67] First, the silicon wafers were washed with ethanol and dried. A dilute solution of Ti5E (5 mol of $TiCl_4$ + 5 mol EtOH) was used. In order to obtain a homogenous, dense layer of TiO_2, we used the following solution: 9.422 g of EtOH + 0.430 g of Ti5E + 0.147 g of H_2O. Silicon wafers were then dip-coated in this solution at a speed of 1.62 mm s^{-1}, temperature of 20 °C and a humidity rate less than 5%. After coating, the samples were calcined at 300 °C for 1 hour. The presence of anatase phase was controlled based on the presence of the (101) reflection in the XRD pattern.

Gold samples. The surfaces constituted of glass substrates (11 mm × 11 mm), coated successively with a 50 Å thick layer of chromium and a 200 nm thick layer of gold. The gold coated substrates were annealed in a butane flame, to ensure good crystallinity of the top-most layers, and rinsed in a bath of absolute ethanol for 15 min before adsorption.

Preparation of solutions

Six different solutions were prepared using sophorolipid powder. Three of them were made at 5 mg mL^{-1} and three more of them at 50 mg mL^{-1}. To obtain a pH 4 solution, adjustments were made with HCl solution at 1 mol L^{-1}, and for pH 11 solution, NaOH solution at 1 mol L^{-1} was added. The solutions were referred to as *X*, *Y*, where *X* is the concentration in mg mL^{-1} and *Y* is the pH value: 5.4; 5.6; 5.11; 50.4; 50.6 and 50.11. All solutions were clear except for the 50.11 solution, which was slightly turbid, the reason for which has been reported elsewhere.[60]

Dip-coating

The dip-coatings were achieved using dip-coating equipment "ACEdip" from Solgelway (www.solgelway.com). If non-specified, all dip-coatings were made at 20 °C with a humidity rate of 25% and a speed of 1 mm s^{-1}.

Characterizations

AFM images of dried surfaces were recorded using a MultiMode 8-HR AFM microscope from Bruker Instruments Inc. To avoid tip and sample damages, topographic images were taken in the QNM Air mode. We used the SCANASYST-Air tips from Bruker (resonance frequency 70 kHz, force constant 0.4 N m^{-1}, tip radius 2 nm). Images were obtained at a constant speed of 1 Hz with a resolution of 512 lines and 512 pixels each. The raw data were processed using the imaging processing software NanoScope Analysis, mainly to correct the background slope between the tip and the surfaces. The thickness measure errors were obtained after estimating the thickness of the films on three different images obtained from the AFM experiments – the values presented were mean values and the errors were calculated as the largest difference between these values and actual measurements. The thickness was estimated using AFM after gently scratching the film and measuring the depth of the scratch. The given surface roughness was calculated as the RMS (root mean square) using a formula (eqn (1)):[68]

$$\mathrm{RMS} = \sqrt{\frac{1}{n}\sum_{i=1}^{n} y_i^2} \qquad (1)$$

where *n* is the amount of equally spaced points along the trace and y_i is the vertical distance from the mean line to the *i*th data point. The values reported in this study were averaged over the entire surface using "Image Roughness" function of the Multimode Nanoscope Analysis 1.5 software.

The adhesion signal was obtained simultaneously with the topographic signal when performing the peak force tapping mode measurements. The adhesion signal (Young modulus) was measured by comparing the attraction forces between the tip and the surface during the approach and retraction phase of the tapping mode. As the cantilever approaches the surface, initially the forces are too small to give a measurable deflection of the cantilever, and it remains undisturbed. At some tip-to-sample distance, the attractive forces overcome the cantilever spring constant, and the tip jumps to contact the surface. Once the contact is established, the tip remains on the surface as the separation between the base of the cantilever and the sample decreases further, causing a deflection of the cantilever and an increase in the repulsive contact force. As the cantilever is retracted from the surface, the tip remains in contact with the surface due to some adhesion, and the cantilever is deflected downwards. Scanning electron microscopy (SEM) was performed on Hitachi S-3400N SEM operated at 5 keV. For each sample, we analyzed five images with ImageJ to obtain the quantitative data. These data have been taken from five images of each sample: one made at the very center of the film and the four other around this position (as displayed in Fig. S1, ESI†) to avoid the border effect. The surfaces of patches were calculated from the images in ImageJ and the data presented were a mean value of what was determined. To estimate the density of patches, the number of patches was determined using ImageJ,[69] and the values were extrapolated to get the estimation on 1 mm^2 area. Contact angle measurements were executed using a Krüss DSA30 goniometer (in sessile drop mode). The volume deposited for each solvent was 2 μL. The images of the drops were recorded using a Stingray F-046 B/C camera of AVT and the results were analyzed using DSA4 software.

Results and discussion

Effect of pH on sophorolipid surface assembly

We have investigated the influence of pH and sophorolipids concentration upon self-organization on a planar silicon surface. In Fig. 2, we have shown AFM images obtained from the samples dip-coated in 50 mg mL^{-1} solution, whereas Fig. S1b (ESI†) presents the control, sophorolipid-free, AFM images acquired at the same resolution. The SEM images of all the samples, displayed in Fig. S2 (ESI†), show an area that is 5-times larger than the one observed using AFM, justifying homogeneity of the assembly on the surface.

The SEM images of Fig. S2 (ESI†) have shown that the surface organization of the molecules differs depending on the pH of the solution during dip-coating. At pH 4, a continuous organization within the film and formation of a two-dimensional network was

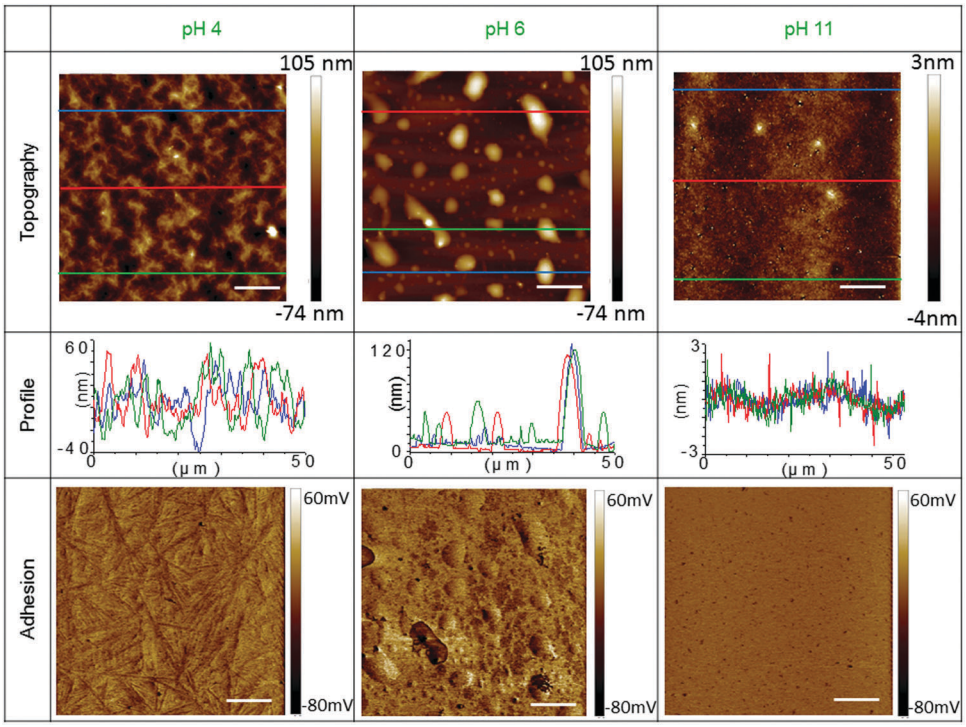

Fig. 2 AFM images from dip-coated solutions (50 mg mL^{-1}) at different pH on silicon samples. Scale bars represent 10 μm (withdrawal speed: 1 mm s^{-1}), color scales were same for every pH.

observed. On maintaining pH around 6, at which partial ionization of the fatty acid occurs, isolated aggregates were observed, while at pH 11, the film appears to be homogeneous. AFM measurements have given better insights into each surface pattern. Fig. 2 shows the topography and adhesion images obtained for the solutions dip-coated on silicon wafer at 50 mg mL^{-1} for three different pH values at a withdrawal speed of 1 mm s^{-1}. The topography and profile obtained from those images indicate the network organization and/or the height of the aggregates. At pH 4, the difference of heights in the network ranges from 60 nm to −40 nm. The top-layer appears to be composed of a tight network of intertwined needles, the size of which is estimated to be 7.5 μm ± 0.6 μm in length and 0.6 μm ± 0.1 μm in cross section. The adhesion image has confirmed similar surface chemistry of the entire sample, thereby indicating good chemical homogeneity and no rupture in the sophorolipid film. For comparison, both the height and adhesion images of the bare silicon substrate are given in Fig. S1b (ESI†): the image displaying height indicates a standard feature-less substrate, although a closer look (adhesion image in Fig. S1b and zoomed *z*-profile in Fig. S1c, ESI†) shows a highly heterogenous surface characterized by a number of defects with a rugosity RMS = 3.13 nm, in contrast to the observation upon deposition of the sophorolipid layer. The AFM image taken at pH 6 exhibits the presence of large aggregates, thereby confirming the SEM data in Fig. S2 (ESI†). There are 2 types of aggregates: the larger ones, which can be seen by SEM (dark circles in Fig. S2, ESI†), and some smaller ones that appear only after AFM analysis. As observed from AFM, the larger aggregates have an average height of 200 nm ± 7 nm and an area around 16 μm^2 ± 3 μm^2, while the smaller ones have an average height of 40 nm ± 5 nm and an area around 3 μm^2 ± 1 μm^2. At pH 11, topography and profile have confirmed the homogeneity and smoothness of sophorolipid film (the difference in height goes from −1 nm to 1 nm with small aggregates of 4–5 nm height). The topography has given insights into fine organization of the film while adhesion has given information on surface chemistry whereas the surface self-organization differed with the pH of the solution (fibrillar network, aggregates or homogeneous layer). The homogeneous adhesion signals recorded throughout the images have shown that for any pH, the sublayer is always composed of the same compound, which we assume to be the sophorolipid. AFM also gives information about the thickness of the organic layer. It appears that under acidic/neutral conditions, thickness was around 40–55 nm (42 nm ± 1 nm at pH 4 and 53 nm ± 1 nm at pH 6), whereas at pH 11, the sophorolipids film was sensibly thicker (235 nm ± 5 nm).

It has been shown in previous studies that whenever acidic sophorolipids form micelles, they adopt a different organization relative to the pH.[56,60–62] For pH < 5, sophorolipids form neutral spheroidal micelles,[61] while for 5 < pH < 7, micelles interact with one another due to negative charge coming from the partial deprotonation of the carboxylic acid.[61,62] Finally, for pH > 8, small spheroidal micelles and platelets to some extent are detected using combined SAXS and cryo-TEM.[60] In some cases, acidic sophorolipids form twisted ribbons under acidic pH conditions.[55,58] However, this was not the case for the compound used in the present study, which only formed a

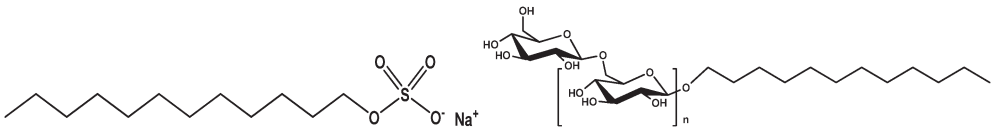

Fig. 3 Schemes of SDS (left) and APG (right).

stable micellar solution. In a recent study,[66] we have given the conditions for a micellar *vs.* fibrillar stability of sophorolipids in water at acidic pH. We were able to show that a standard batch of acidic non acetylated monounsaturated sophorolipid generally formed micelles in water, unless 15 wt% of the saturated form contaminated the batch. Fibers were also observed for highly pure (100%) samples.

In order to show that the pH-dependent surface self-organization effect is truly attributable to the pH-dependent self-assembly properties of sophorolipids, we performed similar control experiments using two amphiphiles (Fig. 3) with no pH-responsive behaviour but with similar structural features found in sophorolipids; sodium dodecyl sulfate (SDS) has a long aliphatic chain and a negatively-charged sulfate polar headgroup, and thus mimics the carboxylate group of sophorolipids in the neutral/basic pH region. A commercial alkylpolyglycoside (APG) amphiphile bearing C10 hydrocarbon chain has also been used to simulate the behavior of sophorolipids in neutral/acidic domain, which was more sensitive to the presence of sophorose headgroup than to the carboxylic acid. The experimental conditions for the surface self-assembly were kept the same (use of Si(111) wafer, and 3 solutions for each amphiphile prepared at pH 4, 6 and 11).

Fig. S3, in the ESI,† compares the surface self-organization properties of sophorolipids, SDS and APG at different pH values for initial concentration of solution as 50 mg mL^{-1}. The organization of SDS and APG was not influenced by the pH of the solution. For every pH value, SDS assembled into organized film of filaments, whereas at pH 4, the filaments appeared to be packed tightly together when compared to that at basic pH. This organization was consistent to a previous study conducted by Bernardes *et al.* on mica[70] and has shown that at high concentration over 10 mM, *i.e.* around 30 mg mL^{-1}, SDS formed no dewetting pattern, rather formed a thick and dense deposit. In any case, pH does not seem to affect the nature of the surface structure. On the other hand, APG formed homogeneously distributed isolated patches rather than a fibrous deposit. Their average surface area was 7.7 $\mu m^2 \pm 1.7$ μm^2. It was interesting to note that at basic pH, structure of an APG film seemed to be more densely packed (about 16 200 patches per mm^2) than at acidic pH (about 4000 patches per mm^2 at pH 4), but the overall surface organization was the same at all pH values. These two tests performed on control molecules confirmed that the evolution of sophorolipids self-assembly onto silicon wafer arises from the pH-dependence of self-assembly properties of this molecule,[56] and that these were not artifacts generated by possibly different wettability of silicon under different pH conditions.

Previous studies by Faustini *et al.*[71] have shown that experimental conditions are critical during dip-coating, and in particular the withdrawal speed (ws): at very low and very high ws, 0.01 mm s^{-1} and 10 mm s^{-1} respectively, the thickness of the film was supposed to be the highest, while a speed in the range 0.1–0.5 mm s^{-1} should help to achieve the thinnest film deposition. Initial experiments were performed at 25 °C with a relative humidity of 25% and a ws of 1 mm s^{-1}. Effect of ws, temperature and humidity during the dip-coating process were then investigated. Fig. 4 has shown SEM images of a film deposited from acidic sophorolipids obtained at three different speeds (at pH 4 and pH 6). The SEM images obtained at standard 1 mm s^{-1} have also been displayed for comparison purposes.

The SEM images show that the nature of surface assembly obtained after dip-coating does not depend on the speed. At pH 4, a two dimensional fibrous network was obtained for each

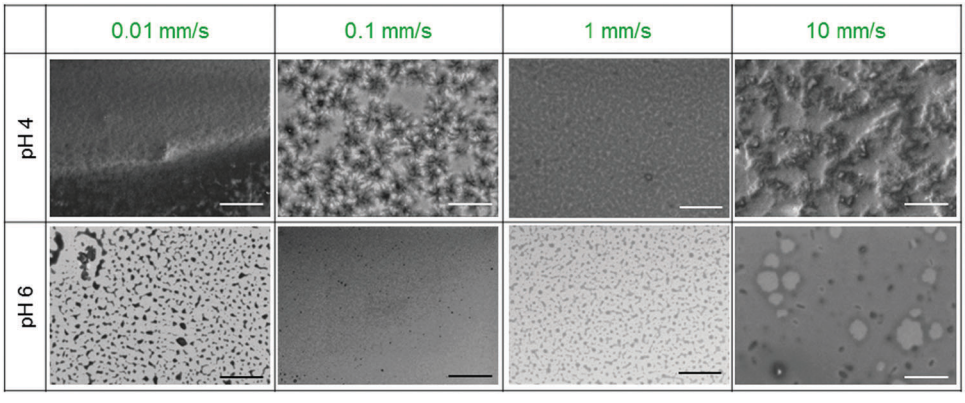

Fig. 4 SEM images indicating the influence of dip-coating withdrawal speed on the surface assembly of sophorolipids on silicon samples. Scale bars represent 50 μm.

speed, whereas the main difference occurred due to the thickness of the film. For intermediate speed, 0.1 and 1 mm s^{-1}, the film obtained with solution of 50 mg mL^{-1} was 2.1 ± 0.5 nm and 1.4 ± 0.2 nm thinner, respectively than the film retrieved at 0.01 mm s^{-1} with a thickness of 4.3 ± 0.5 nm. On contrary, at pH 6, isolated aggregates were observed for all ws tested but the average area of those aggregates differed; at 0.01 mm s^{-1}, the mean area was around 17 μm^2 (with a large distribution from 1 to 30 μm^2, Fig. S4a, ESI†), while at 1 mm s^{-1}, the average area was 12 μm^2 (with a tight distribution from 1 to 10 μm^2) (Fig. S4b, ESI†). Based on SEM images, surface density of the patches can be estimated. At 0.01 mm s^{-1}, the average density was found to be 2825 aggregates per mm^2. At 0.1 mm s^{-1}, the average density was determined as 910 aggregates per mm^2, and at 1 mm s^{-1}, the average density was 11 000 aggregates per mm^2. At a very low speed (0.01 mm s^{-1}), the film formation was ruled by the capillary regime wherein solvent evaporation was faster than the motion of the drying line.[71] The film was then thick and the molecules could adopt less energetic organization on the surface. On the contrary, at high withdrawal speed (10 mm s^{-1}), the film formation was governed by the draining regime. This phenomenon can be described by Landau–Levich equation to predict the film thickness.[72] It has been demonstrated that the presence of surfactants in an aqueous solution during dip-coating led to thicker films (thickness 60 percent higher with surfactants in solution).[73] The sophorolipid film obtained within the draining regime was thick and rough; the latter phenomenon being due to a competition between adhesion and gravity during the dip-coating process. Moreover, it was complicated to have a good control on the film formation in water because of the high surface tension of this solvent.[71] Therefore, at high ws, we cannot control the self-assembly. We have observed large and inhomogeneous patches but they were composed of fibrillar domains at pH 4, while aggregates persisted on the surface at pH 6. In summary, using a withdrawal speed of 1 mm s^{-1} was found to be a good compromise between optimal film thickness and the control of self-assembly on the surface.

The influence of temperature and humidity rate was also investigated with two supplementary experiments. In the ESI,† we have compared the SEM images obtained at pH 4 and pH 6 at 25 °C and 66 °C (Fig. S5, ESI†), while in Fig. S7 (ESI†) we compare the effect of relative humidity (RH) 25% *versus* 96%, at constant temperature (24 °C). At 66 °C a faster drying process was expected; however, at the chosen withdrawal speed 1 mm s^{-1}, we did not find significantly different surface self-assembly effects. At pH 4, the system was still fibrous. Their presence was confirmed by AFM adhesion images (Fig. S6, ESI†). At pH 6, temperature does not affect the nature of the surface aggregates, which can be assumed as micron-sized spheroidal domains are still observed. However, the average surface area is smaller (around 70% less than at 25 °C) and above all, an alignment of the domains parallel to the withdrawal direction is systematically observed (Fig. S5, ESI†).

When the relative humidity was increased up to 96%, evaporation rate of water decreased,[74] thus keeping the hydrophilic headgroups of sophorolipids hydrated.[75] At pH 4, the surface self-assembly was more homogeneous with locally concentrated aggregates of matter of undefined shape with the disappearance of the fibrous structure (Fig. S7, ESI†). At pH 6, the surface organization shows an interconnected network of sophorolipid aggregates rather than individually well-separated domains. However, the nature of the aggregates was comparable at RH 25% and 96%. Humidity, rather than temperature, seemed to play an important role in the surface molecular arrangement. It can be believed that higher hydration degree of the sophorolipids throughout the dip-coating process was the main driving force that influenced the assembly. In fact, temperature variation experiments have shown (Fig. S5, ESI†) that variations in the evaporation rate may affect the local order but not the nature of the assembly. For this reason, at high relative humidity, where two effects play together, among slower evaporation rate of water and higher hydration degree of sophorolipids, the former might play a minor role and the latter may have a stronger influence. Hydration/dehydration effect on lipid self-assembly was well-known in bulk solution,[76,77] and this phenomenon also contributed to impact the nature of the local assembly of sophorolipids on the silicon surface. Another possibility of higher humidity may result in the change of surface chemistry. Indeed, with a slow evaporation rate and high hydration of head groups, the diffusion of sophorolipids in the aqueous layer increases and the intermolecular bond is favored. Higher humidity also leads to higher vapor pressure, which may alter the native oxide layer composition of silicon due to reaction between the –OH surface group and the ambient water.[78]

Effect of surface type on sophorolipid assembly

In order to investigate the role of surface chemistry upon self-assembly of sophorolipids, three original solutions (pH 4, pH 6 and pH 11) were dip-coated on three different surfaces. Silicon(111) wafers were compared to bare gold and silicon(111) wafer coated with a titanium dioxide anatase thin layer. The control AFM images for gold and TiO_2 have been provided in Fig. S1b (ESI†) that justify the standard homogeneous flat surface having a roughness of RMS = 2.14 nm and 1.37 nm for gold and TiO_2, respectively. The initial conditions of dip-coating were the same for all substrates: ws = 1 mm s^{-1}, T = 25 °C and RH = 25%. The AFM images of these films are displayed in Fig. 5 and the SEM images have been depicted on Fig. S8 (ESI†). Gold was chosen because it is considered to be chemically inert and does easily not chemisorb molecules,[79] although recently some research groups have shown that bulk gold can have catalytic activity when activated.[80] The titanium dioxide is a good compromise between enhancement of hydroxyl group and its affinity towards carboxylic acids.[81–83]

The SEM images taken for each surface showed different surface organizations depending on the substrate chemical composition. As one can see, when the solutions are dip-coated on gold, the long-range texture seems to be constituted by a homogenous deposit with dispersed, and that at any pH; AFM images, acting as a local probe, in fact show that the film

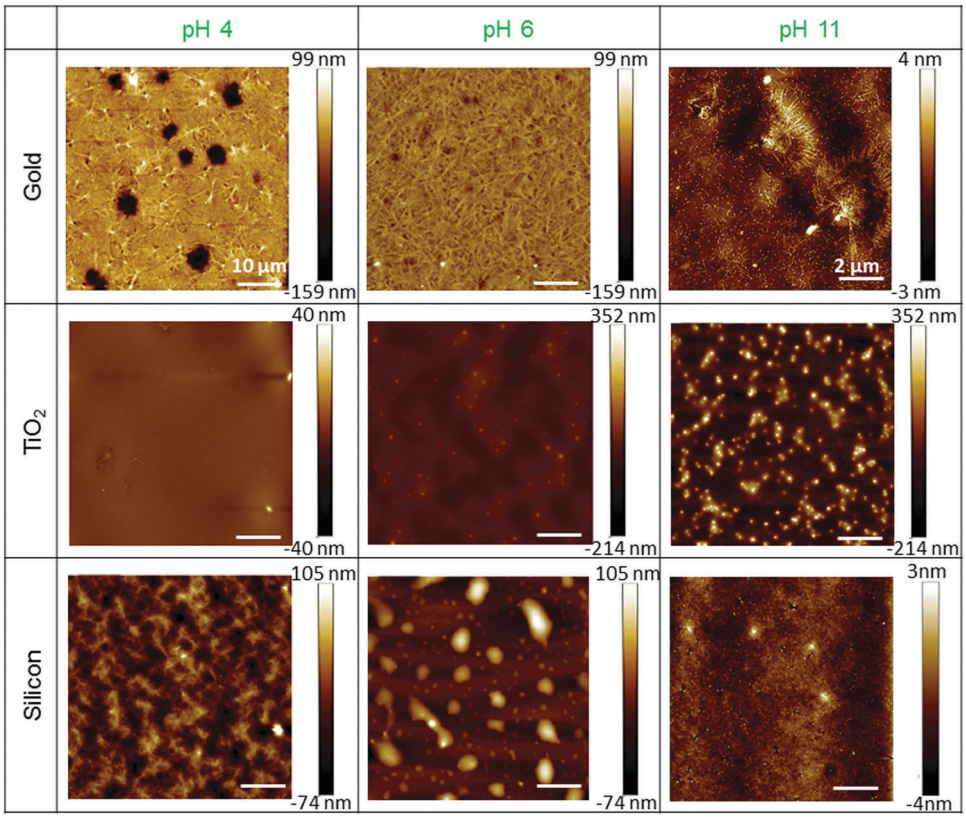

Fig. 5 Topography AFM images from dip-coated solutions at different pH onto different substrates (gold, TiO_2, silicon). Scale bars represent 10 µm, except for the image on gold at pH 11 where the scale bar represents 2 µm. For direct comparison, we have reported images taken on silicon and previously presented on Fig. 4.

on gold is constituted of entangled filaments at any pH and the white spots observed in the SEM images actually represent holes in the structure. AFM gives a vision of the surface organization in detail. There was a homogeneous layer upon which there were some needles: the longer ones (2–3 µm) appeared to be generated from a nucleation center, while the shorter ones (30–100 nm) were spread randomly on the organic layer. The cross-section of the needles was 40 nm ± 9 nm. On the layer of titanium dioxide, pH seems to have a weak influence. At pH 4, the film is rather homogeneous, while at pH 6 and pH 11, the film obtained constitutes a homogeneous layer of sophorolipids upon some isolated aggregates randomly observed. The main difference was the size of these aggregates: from the AFM images, we measured that at pH 6, the average size was around 0.60 $\mu m^2 \pm 0.21$ μm^2 and at pH 11, the average size was around 0.33 $\mu m^2 \pm 0.15$ μm^2. The size differences could be explained by the presence of carboxylate groups at basic acid creating charge repulsions during the aggregation, thus leading to smaller aggregates. These observations indicated that surface chemistry was also relevant while studying the self-assembly of organic molecules on flat surfaces. All the results collected have been tabulated in Table 1.

To rely more on quantitative data and to better understand the sophorolipids self-assembly in relationship with the surface properties, we have evaluated the wettability and surface energy profiles for all supports used, and the results are presented in Fig. 5. First of all, contact angle measurements of water were used to evaluate the wettability of the surface.[84] Higher the angle, more hydrophobic is the surface. The measurements were reported with drop images for each sample in Fig. S9 (ESI†).

Table 1 Collection of AFM data for all the sophorolipids films observed

	pH 4	pH 6	pH 11
Gold	Needles entangled	Needles entangled tighter	Isolated needles: length 2–3 µm/30–100 nm cross section 40 nm
TiO_2	Homogeneous film	Aggregates: area around 0.60 μm^2	Aggregates: area around 0.33 μm^2
Silicon	Intertwined needles: length 7.5 µm cross section 60 nm	Aggregates, 2 types: large: area 16 μm^2 and height 80 nm small: area 3 μm^2 and height 40 nm	Homogeneous film

The angles reported were a mean value obtained after measurements on 4 drops on each sample. Within the framework of our experimental conditions, we determined a contact angle of 69° ± 4° on bare gold in accordance with a previous study,[85] 52° ± 6° on titanium dioxide anatase layer, and 43° ± 4° on silicon wafer. If titanium dioxide was known to be highly hydrophilic, the value we have determined was actually coherent to the values reported in the literature[86] for a non-model surface that contains environmental impurities. These data have indicated that the gold surfaces, as prepared in these experiments, were the most hydrophobic samples and silicon wafers were the most hydrophilic. This difference of wettability might be a first explanation for the differences observed with AFM.

Effect of surface energy on sophorolipid assembly

The second set of experiments aims at determining the surface energy of each sample and more precisely, the contribution of apolar and polar components. Good–Van Oss's approach using glycerol, formamide and diiodomethane as wetting solvents was applied.[87,88] To determine the values of each component of the solid surface energy, we used eqn (2):

$$\gamma_L(1+\cos\theta) = 2\left[\sqrt{\gamma_S^{LW}\gamma_L^{LW}} + \sqrt{\gamma_S^{+}\gamma_L^{-}} + \sqrt{\gamma_S^{-}\gamma_L^{+}}\right] \qquad (2)$$

where θ is the contact angle between the solvent and the surface (in degree), γ_L is the total surface tension of the liquid, γ_L^{LW} and γ_S^{LW} are the Lifshitz–van der Waals (or dispersive) component for the liquid and solid surface tension respectively. γ_L^- (γ_S^-) is the basic (Lewis) component of surface interaction, that is the electron donor component for the liquid (and solid), and γ_L^+ (γ_S^+) is the acid (Lewis) component of surface interaction, that is the electron acceptor component for the liquid (and solid). Two contact angle measurements (θ) and the surface tension data for all liquids are given in Table S1 (ESI†).[89,90] The surface energy data calculated for each samples using eqn (2) have been collected in Table 2 and the contribution of the separated components is plotted in Fig. 6.

According to the plots in Fig. 6, the samples could easily be sorted out by increasing surface energy. In the present study, gold surfaces have the lowest surface energy while silicon has the strongest surface energy contribution. The values of total surface energy were coherent to the contact angle observations. Silica, being the most hydrophilic surface, is expected to have the highest surface energy,[94] and the values obtained in this work are in good agreement with those reported in literature. The data reported by Knorr *et al.*[91] on gold composites are in the same range as our study (Table 2). Unfortunately, to the best of our knowledge, there is no report on electron donor/acceptor contributions to surface energy for titanium dioxide. Kilpadi *et al.* have reported data on passivated titanium samples[92] exhibiting an outer layer of dioxide, which can be taken as references. The data on silicon were compared to previous studies conducted on silica by Chibowsky[93] and Gonzalez-Martin[88] since the native silicon have always exhibited a thin layer of silica on the surface. Herein, silicon wafer as an effective SiO_2 sample is discussed below.

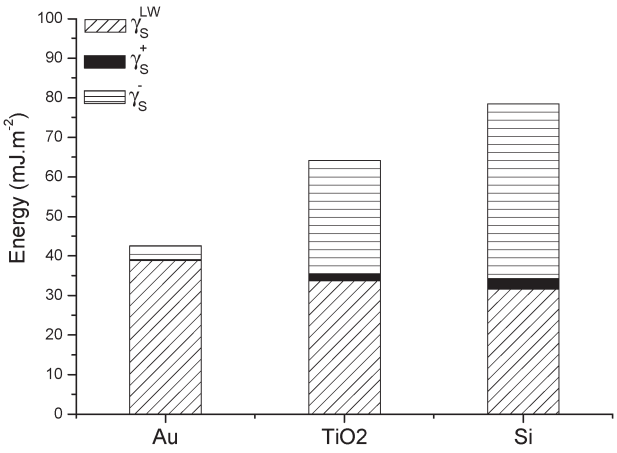

Fig. 6 Total surface energy for each surface, determined by measuring contact angle with diiodomethane, glycerol and formamide.

Roughness could certainly have an effect on the surface self-assembly and patterning of the substrates, but to the first approximation, its effect has been implicitly taken into account in the proposed study for the following reasons: (1) the first part of this study has employed only one type of substrate, silicon, for all experiments on lipids, including pH change, variations in the RH, dip coating withdrawal speed and lipid type (sophorolipids, alkylpolyglycoside and SDS). Therefore, one can reasonably assume that roughness was invariant among all substrates, thus having a systematic impact on all the samples. The same arguments hold true for the pH changes variation performed on gold and anatase substrates. (2) Based on the comparison between different substrates, the effect of roughness was exhibited on the polar electron-donor component of the surface energy (which increased with decreasing roughness), as reported by Yan *et al.*[95] By comparing the non-dispersive contributions to surface energy, which concern the polar components considered as short-range superficial interactions, in silicon, gold and anatase substrates, roughness is implicitly taken into account. (3) The surface roughness of the bare substrates evaluated by AFM was between 1 < RMS (nm) < 3, and it was comparable to the size of a single monolayer of sophorolipids. Considering the fact that the sizes of surface aggregates and fibrils were in the order of μm, it can be assumed that this parameter had little influence in this specific study.

According to data in Table 2, dispersive and electron acceptor components were comparable for all materials around

Table 2 Values of surface energy components calculated (in mJ m^{-2}) from Van Oss's equation and the contact angle measured (see Table S1, ESI)

				Reference data			
Surface	γ_S^{LW}	γ_S^+	γ_S^-	γ_S^{LW}	γ_S^+	γ_S^-	Ref.
Gold	38.9	0.2	3.4	30	1.2	7.8	91
Titanium dioxide	33.7	1.8	28.7	40–42	—	—	92
Silicon	31.6	2.7	44.1	32–43	0.2–5	32–62	88 and 93

30–40 mJ m^{-2} and below 3 mJ m^{-2}, respectively, but the electron-donor component was sensibly different for gold, TiO_2 and silica, where the latter material has the higher value (44.1 mJ m^{-2}). For this reason, a hypothesis has been developed in such a way that the differences in terms of surface self-assembly observed by SEM and AFM might depend on γ_S^-. This conclusion was not unexpected because of the difference in terms of the surface chemistry for these materials. The Point of Zero Charge (PZC) for SiO_2 was 2, IsoElectric Point (IEP) of TiO_2 was in the vicinity of 6 but it may actually vary between 3 and 7 according to the crystalline phase, method of preparation and surface roughness in thin films. Gold, on contrary, had neither PZC nor IEP.[96,97] Given the fact that silica had the lowest PZC, its surface could reasonably be considered to be rich in SiO^- groups (enhancing the γ_S^- component of surface energy) at different extent according to the solution pH. At pH 4, the sophorolipids solutions form micelles that are not charged[56] and silica can be considered as poorly charged, while at pH 6, the sophorolipids solutions are characterized by increasingly charged micelles undergoing electrostatic repulsion,[56,62] whereas silica can be practically considered to be fully charged. Moreover, in case of TiO_2, given the higher IEP, much difference in terms of surface charge between pH 4 and pH 6 must not be expected. At pH 4 for SiO_2 and pH 4 and at pH 6 for gold, the SEM and AFM data have shown the formation of entangled network of fibers, probably forming from a nucleation/growth mechanism; moreover, a phenomenon that can most likely be ascribed to dewetting seems to occur on silica at pH 6, practically under all conditions explored in terms of withdrawal speed, temperature and relative humidity. Additional insight in terms of surface energy can help understand these different effects.

Discussion

Sophorolipids form two main types of surface aggregation patterns, a fibrillar network and a surface circular patches. The former can be explained by the ability of sophorolipids to self-assemble into crystalline fibers, as described by previous authors[55,58] and recently explained by us;[63] the latter strongly recalls dewetting phenomena of surfactant solutions on surfaces, which depend on the autophobic effect,[31] probably driven by the local formation of a self-assembled lipid monolayer on the surface.[32,36] In the following paragraphs we tried to rationalize both possibilities.

Conditions for dewetting phenomena can be estimated from the sign of the spreading coefficient S for each sample (eqn (3)), knowing that S was an empirical parameter calculated from surface tension data:

$$S = \gamma_S - \gamma_L - \gamma_{\frac{L}{S}} = \gamma_L(\cos\theta - 1) \qquad (3)$$

where γ_S, γ_L, and $\gamma_{L/S}$ are the surface tension values of the solid, sophorolipids solution and the interfacial tension of sophorolipids and solid, respectively.[98] In literature, it has been reported that the sophorolipids could lower the surface tension of water from 72.8 mJ m^{-2} to 40–30 mJ m^{-2}.[44] In the present systems, for all samples, we found that $S < 0$ for each sample, in principle, a dewetting phenomenon occurred during the drying of the sophorolipids film.[99] In addition, Lee *et al.*[100] have demonstrated that dispersive forces would stabilize the film while polar ones would induce dewetting. There were two dewetting processes that could happen: spinodal dewetting or heterogeneous nucleation.[101] It is commonly admitted that nucleation occurs in the early stage of dewetting and spinodal dewetting is promoted for thin films.[101,102] On gold samples, the values of polar components ($\gamma^+ + \gamma^-$) were ten times lower than those of the apolar one (γ^{LW}); hence, following Lee's idea, it indicated that gold surface exhibits a strong stabilizing force towards the film. The SEM images showed the beginning of the dewetting process through the heterogeneous nucleation (white spots) stopped before the growth of holes because of the stabilizing force of gold surface. This was also confirmed by the random distribution of holes characteristic of heterogeneous nucleation according to Seeman.[101] This organization was stable because the gold surface was not sensitive to pH changes. On utilizing titanium dioxide, the contributions of polar and apolar components were rather comparable. The dispersive contribution was slightly higher than the polar ones, and hence, on this surface, dewetting was supposed to be less effective; homogeneous layers were then obtained. The aggregates observed at pH 6 and pH 11 might be due to the presence of different objects in solution with the micelles: interacting micelles (larger than the usual one) at pH 6 and the platelets at pH 11.

On SiO_2 samples, the polar component was slightly higher than the apolar one. The dewetting was then expected. But as one can see in Fig. 5, at pH 4 the dewetting was limited, while at pH 6, we observed a partial dewetted film. The other interactions have to be considered because of the high sensitivity of silica layer towards pH changes. As it has been shown in this study, on SiO_2 at pH 4, there was a thin sophorolipids layer, and the SEM images show a network similar to the one observed in the surface assembly of block copolymers.[20,103] By definition, the spinodal decomposition was a clustering phase change from a homogeneous matter that separated spontaneously into two phases due to a small fluctuation of density or composition.[104] Two other phenomena could explain the phase separation within a film. First, the partial trapping of solvent (*e.g.* ethanol used to wash the substrates) and water (during the dip-coating) as it has been demonstrated by Wong *et al.* can promote phase separation, as shown for block copolymer film for PHPMA on silicon.[105] Second, Marangoni effect due to the local difference of sophorolipids concentration can induce a fluctuation of matter in the film. Fell *et al.*[106] have demonstrated that there was a gradient of surfactant on the receding side of their cylinder (analog to the front line during dip-coating) and this gradient was even stronger when the surfactants concentration was above cmc because the diffusion was lower. At pH 6, we observed a strong dewetting effect as expected, due to the slow process involved to achieve complete drying of the sophorolipids film. Several studies[107,108] have demonstrated that polymer could dewet upon a polymer–

polymer surface or when deposited on polymer brush with the same formula. More recently, Xue *et al.*[109] have shown that this autophobic dewetting was particularly happening when the film was in the presence of a good solvent vapor. In the present case, slow drying at pH 6 could lead to the water adsorption onto the outer layer of the film. This induced a difference of entropy between the molecule in contact with the vapor and the ones close to the surface, thereby creating a new interface where the top molecules could slide upon the sophorolipids layer to form the final aggregates (or droplets). Finally, the sophorolipids film was thicker at pH 11 than that at acidic pH, and the samples were the fastest to dry during dip-coating, and hence no spinodal dewetting was predicted for this solution. Kassal *et al.* have shown a correlation between surface energy, polarity and pH sensing.[110]

Our hypothesis is that the values of γ^- and γ^+ are dependent of the pH. At pH 4, because we are close to the PZC of SiO_2, the surface was neutral and the effective values of γ^- and γ^+ were lower than the ones calculated. There was no dewetting probably because the sophorolipids film assembly was ruled by γ^{LW}. The formation of fibers, which may seem quite odd if one considers the stable micellar phase in solution, is actually not surprising as acidic sophorolipids have shown to form both micelles[56,62] and fibers in water under acidic pH conditions.[55,58] At the moment, the conditions that favor one phase over the other were only partially known[66] and a tentative explanation at the molecular level in terms of surface–sophorolipid interactions favouring fiber formation would be highly speculative. However, we must consider that similar effects have been described for amyloid-β peptides on mica and can undergo a micelle-to-fibril transition as a function of number density of the peptides on the surface, which depends on the deposition and diffusion rates of the peptides. No specific correlation with the surface energy has been proposed in this study.[111]

At pH 6, SiO^- were majorly present on the surface, and dewetting was thus due to higher values of γ^- and γ^+ over γ^{LW}. At pH 11, dewetting was also expected but due to the thickness of the sophorolipids film, this phenomenon was limited. The correlation between aqueous film thickness and dewetting was established for dodecyltrimethylammonium bromide solutions The authors[32] have shown that autophobing, responsible for dewetting, occurred at longer times for thicker films. The evolution of the values of surface energy components was correlated with the changes of contact angle observed when changing the pH of water (without any sophorolipids). The contact angle values decrease (so surface energy increases) with an increase in pH. The observations were enhanced for treated silicon samples because the surface was even more sensitive to the eternal conditions, such as pH, due to higher hydroxyl density.

Finally, as a general observation we are tempted to state that sophorolipid assembly and patterning depended on γ_S^{LW} *vs.* γ_S^- balance of each surface. When dispersive forces were predominant, sophorolipid packed into fibrillar aggregates, while polar components contributed to stabilize micellar aggregates, autophobing and eventually dewetting. Additional experiments would be required to understand the sophorolipid–surface interactions and its effect on autophobing effect that gives rise to dewetting.

Conclusion

In this study, we investigated the surface self-assembly properties of acidic sophorolipids, a bolaform microbial glycolipid, according to the chemical nature of the support and pH of the solution. Sophorolipids generally form micelles in water but the nature of the micelle aggregates and possible non-micellar morphologies like platelets and twisted fibers have also been reported according to pH. We have selected three different substrates namely gold, silicon and TiO_2 anatase, wherein silicon has been utilized as a SiO_2 native oxide layer. The dispersive, electron donor and electron attractor surface energy components have systematically been determined for all substrates by Good–Van Oss's approach using glycerol, formamide and diiodomethane as wetting solvents. We have found that when gold was used as the substrate, where surface energy of is dominated by dispersive (γ_S^{LW} = 38.9 mJ m^{-2} > γ_S^+, γ_S^-) components, sophorolipids spontaneously assembled into entangled needles at all pH values (4, 6 and 11). When TiO_2 anatase, characterized by a high dispersive (γ_S^{LW} = 37.7 mJ m^{-2}) surface energy component in addition to a higher electron donor component compared to gold (γ_S^- = 28.7 mJ m^{-2}) and still a small electron acceptor component (γ_S^+ = 1.8 mJ m^{-2}), is used as a substrate, we observe a relative homogeneous sophorolipid layer, although with an increasing amount of ill-defined aggregates with increasing pH. Finally, when SiO_2, characterized by larger γ_S^- (=44.1 mJ m^{-2}) component than γ_S^{LW} (=31.6 mJ m^{-2}) and a still low γ_S^+ (=2.7 mJ m^{-2}), is used as a substrate, we find that pH has a strong influence and three different sophorolipid surface assemblies can be described. At pH 4, we observed the formation of an entangled network of needles, having an average length of 7.5 μm and a cross section of about 60 nm. At pH 6, dewetting occurs and a patterned surface of small (area: 3 μm^2; height: 40 nm) and large (area: 16 μm^2; height: 80 nm) aggregates is observed; at pH 11, we observe the formation of a homogeneous sophorolipid layer. We then considered that surface chemistry and pH-dependent behaviour of sophorolipids can be ascribed to γ_S^{LW} *vs.* γ_S^- balance of each surface. This can also determine whether or not dewetting is favoured, for instance, γ_S^- evolution with pH strongly depended on the surface chemistry of each material and in particular to the specific values of IEP and PZC (SiO_2, TiO_2) or to their absence (gold). The low PZC (2) of SiO_2 can make the self-assembly of sophorolipids on this material extremely sensitive to pH and to the evolution of γ_S^-, while higher and less defined IEP (3–7) of TiO_2 makes the pH-dependent behaviour of this substrate less marked, although present, due to the comparable values of γ_S^{LW} and γ_S^-. Finally, gold has no pH-dependent surface chemistry, making γ_S^{LW} *de facto* drive the self-assembly of sophorolipids.

Acknowledgements

The authors would like to thank the University Pierre et Marie Curie for the funding of the ATER position for this study.

References

1 V. D. Ta, A. Dunn, T. J. Wasley, J. Li, R. W. Kay, J. Stringer, P. J. Smith, E. Esenturk, C. Connaughton and J. D. Shephard, *Appl. Surf. Sci.*, 2016, **365**, 153–159.
2 Y. Xia, D. Qin and Y. Yin, *Curr. Opin. Colloid Interface Sci.*, 2001, **6**, 54–64.
3 H.-P. Chou, M. A. Unger, A. Scherer and S. R. Quake, *Proceedings of the Solid State Actuator and Sensor Workshop*, Hilton Head, South Carolina, 2000.
4 J. Voldman, M. L. Gray and M. A. Schmidt, *Annu. Rev. Biomed. Eng.*, 1999, **1**, 401–425.
5 D. Nyamjav and R. C. Holz, *Langmuir*, 2010, **26**, 18300–18302.
6 X. Zhang, F. Liu and H. Li, *Materials*, 2016, **9**, 121–128.
7 S. Ghosh, D. Kaiser, J. Bonilla, T. Sinno and S. M. Han, *Appl. Phys. Lett.*, 2015, **107**, 72106.
8 P. M. Tessier, O. D. Velev, A. T. Kalambur, J. F. Rabolt, A. M. Lenhoff and E. W. Kaler, *J. Am. Chem. Soc.*, 2000, **122**, 9554–9555.
9 A. Biswas, I. S. Bayer, A. S. Biris, T. Wang, E. Dervishi and F. Faupel, *Adv. Colloid Interface Sci.*, 2012, **170**, 2–27.
10 X. Liu, X. Zhang and Z. Zhou, *Mater. Res. Bull.*, 2016, **79**, 84–89.
11 K. Yung, C. Lee, C. Wong, S. Tam, S. Pang and T. Yue, *J. Electron. Mater.*, 2013, **42**, 3494–3501.
12 I. Kokal, O. F. Göbel, E. J. Van den Ham, J. E. ten Elshof, P. H. Notten and H. T. Hintzen, *Ceram. Int.*, 2015, **41**, 13147–13152.
13 J. Hu, R. G. Beck, T. Deng, R. M. Westervelt, K. D. Maranowski, A. C. Gossard and G. M. Whitesides, *Appl. Phys. Lett.*, 1997, **71**, 2020–2022.
14 H. L. Huang, J. K. Chen and M. P. Houng, *Thin Solid Films*, 2012, **524**, 304–308.
15 L. (Leon) Yuan and P. R. Herman, *Nanoscale*, 2015, **7**, 19905–19913.
16 W. Kern and J. M. Shaw, *J. Electrochem. Soc.*, 1971, **118**, 1699–1704.
17 X. Gao, W. Feng, S. Zhu, H. Sheardown and J. L. Brash, *Langmuir*, 2008, **24**, 8303–8308.
18 M. J. Fasolka and A. M. Mayes, *Annu. Rev. Mater. Res.*, 2001, **31**, 323–355.
19 R. B. Cheyne and M. G. Moffitt, *Langmuir*, 2006, **22**, 8387–8396.
20 J. N. L. Albert and T. H. Epps, *Mater. Today*, 2010, **13**, 24–33.
21 J. Ji, L. Feng, Y. Qiu, X. Yu and M. A. Barbosa, *J. Colloid Interface Sci.*, 2000, **224**, 255–260.
22 H. Yuan, H. Chi and W. Yuan, *Carbohydr. Polym.*, 2016, **147**, 261–271.
23 H.-C. Kim and W. D. Hinsberg, *J. Vac. Sci. Technol., A*, 2008, **26**, 1369.
24 D. E. Angelescu, J. H. Waller, D. H. Adamson, P. Deshpande, S. Y. Chou, R. A. Register and P. M. Chaikin, *Adv. Mater.*, 2004, **16**, 1736–1740.
25 S. H. Kim, M. J. Misner, T. Xu, M. Kimura and T. P. Russell, *Adv. Mater.*, 2004, **16**, 226–231.
26 M. Kimura, M. J. Misner, T. Xu, S. H. Kim and T. P. Russell, *Langmuir*, 2003, **19**, 9910–9913.
27 L. Guo, Y. Jiang, S. Chen, T. Qiu and X. Li, *Macromolecules*, 2013, **47**, 165–174.
28 M. Byun, W. Han, B. Li, X. Xin and Z. Lin, *Angew. Chem., Int. Ed.*, 2013, **52**, 1122–1127.
29 A. Marmur and M. Lelah, *Chem. Eng. Commun.*, 1981, **13**, 133–143.
30 A. B. Afsar-Siddiqui, P. F. Luckham and O. K. Matar, *Adv. Colloid Interface Sci.*, 2003, **106**, 183–236.
31 D. Qu, R. Suter and S. Garoff, *Langmuir*, 2002, **18**, 1649–1654.
32 A. B. Afsar-Siddiqui, P. F. Luckham and O. K. Matar, *Langmuir*, 2004, **20**, 7575–7582.
33 B. Frank and S. Garoff, *Langmuir*, 1995, **11**, 87–93.
34 B. Frank and S. Garoff, *Langmuir*, 1995, **11**, 4333–4340.
35 R. V. Craster and O. K. Matar, *Langmuir*, 2007, **23**, 2588–2601.
36 J. T. Woodward and D. K. Schwartz, *Langmuir*, 1997, **13**, 6873–6876.
37 A. Zelcer, A. Wolosiuk and G. J. A. A. Soler-Illia, *J. Mater. Chem.*, 2009, **19**, 4191.
38 N. Baccile, T. Fontecave, C. Boissière and I. N. A. Van Bogaert, *J. Phys. Chem. C*, 2013, **117**, 23899–23907.
39 D. W. G. Develter and S. J. J. Fleurackers, in *Surfactants from Renewable Resources*, ed. M. Kjellin and I. Johansson, John Wiley & Sons, Ltd, Chichester, 2010, pp. 213–238.
40 I. N. A. Van Bogaert, K. Saerens, C. De Muynck, D. Develter, W. Soetaert and E. J. Vandamme, *Appl. Microbiol. Biotechnol.*, 2007, **76**, 23–34.
41 H. J. Daniel, M. Reuss and C. Syldatk, *Biotechnol. Lett.*, 1998, **20**, 1153–1156.
42 E. I. P. Delbeke, J. Everaert, E. Uitterhaegen, S. Verweire, A. Verlee, T. Talou, W. Soetaert, I. N. A. Van Bogaert and C. V. Stevens, *AMB Express*, 2016, **6**, 28.
43 S. J. J. Fleurackers, *Eur. J. Lipid Sci. Technol.*, 2006, **108**, 5–12.
44 I. N. A. Van Bogaert, J. Zhang and W. Soetaert, *Process Biochem.*, 2011, **46**, 821–833.
45 D. Kitamoto, T. Morita, T. Fukuoka, M. A. Konishi and T. Imura, *Curr. Opin. Colloid Interface Sci.*, 2009, **14**, 315–328.
46 J. N. Sleiman, S. A. Kohlhoff, P. M. Roblin, S. Wallner, R. Gross, M. R. Hammerschlag, M. E. Zenilman and M. H. Bluth, *Ann. Clin. Lab. Sci.*, 2009, **39**, 60–63.
47 D. W. G. Develter and L. M. L. Lauryssen, *Eur. J. Lipid Sci. Technol.*, 2010, **112**, 628–638.
48 S. L. Fu, S. R. Wallner, W. B. Bowne, M. D. Hagler, M. E. Zenilman, R. Gross and M. H. Bluth, *J. Surg. Res.*, 2008, **148**, 77–82.

49 I. A. C. Ribeiro, C. M. C. Faustino, P. S. Guerreiro, R. F. M. Frade, M. R. Bronze, M. F. Castro and M. H. L. Ribeiro, *J. Mol. Recognit.*, 2015, 155–165.

Q10 50 1995.

51 V. K. Morya, C. Ahn, S. Jeon and E.-K. Kim, *Mini-Rev. Med. Chem.*, 2013, **13**, 1761–1768.

52 K. Joshi-Navare, P. Khanvilkar and A. Prabhune, *Biochem.*

Q11 *Res. Int.*, 2013, **2013**.

53 R. D. Ashby, D. K. Y. Solaiman and T. A. Foglia, *Biotechnol. Lett.*, 2008, **30**, 1093–1100.

54 A. M. Shete, G. Wadhawa, I. M. Banat and B. A. Chopade, *J. Sci. Ind. Res.*, 2006, **65**, 91–115.

55 S. Zhou, C. Xu, J. Wang, W. Gao, R. Akhverdiyeva, V. Shah and R. Gross, *Langmuir*, 2004, **20**, 7926–7932.

56 N. Baccile, F. Babonneau, J. Jestin, G. Pehau-Arnaudet and I. Van Bogaert, *ACS Nano*, 2012, **6**, 4763–4776.

57 N. Baccile, J. S. Pedersen, G. Pehau-Arnaudet and I. N. A. Van Bogaert, *Soft Matter*, 2013, **9**, 4911–4922.

58 P. Dhasaiyan, A. Banerjee, N. Visaveliya and B. L. V. Prasad, *Chem. – Asian J.*, 2013, **8**, 369–372.

59 N. Baccile, A.-S. Cuvier, S. Prévost, C. V. Stevens, E. Delbeke, J. Berton, W. Soetaert, I. N. A. Van Bogaert and S. Roelants, *Langmuir*, 2016, **32**, 10881–10894.

60 A. S. Cuvier, F. Babonneau, J. Berton, C. V. Stevens, G. C. Fadda, G. Péhau-Arnaudet, P. Le Griel, S. Prévost, J. Perez and N. Baccile, *Chem. – Eur. J.*, 2015, **21**, 19265–19277.

61 S. Manet, A. S. Cuvier, C. Valotteau, G. C. Fadda, J. Perez, E. Karakas, S. Abel and N. Baccile, *J. Phys. Chem. B*, 2015, **119**, 13113–13133.

62 N. Baccile, J. S. Pedersen, G. Pehau-Arnaudet and I. N. A. Van Bogaert, *Soft Matter*, 2013, **9**, 4911–4922.

63 P. Dhasaiyan, P. Le Griel, S. Roelants, E. Redant, I. N. A. Van Bogaert, S. Prevost, B. L. V. Prasad and N. Baccile, *ChemPhysChem*, 2017, DOI: 10.1002/

Q12 cphc.201601323.

64 L. Zhang, P. Somasundaran, S. K. Singh, A. P. Felse and R. Gross, *Colloids Surf., A*, 2004, **240**, 75–82.

65 N. Baccile, A. S. Cuvier, C. Valotteau and I. N. A. Van Bogaert, *Eur. J. Lipid Sci. Technol.*, 2013, **115**, 1404–1412.

66 P. Dhasaiyan, P. Legriel, S. Roelants, E. Redant, I. N. A. Van Bogaert, S. Prévost, P. Bhagavatula and N. Baccile, under

Q13 revise.

67 M. C. Fuertes, S. Colodrero, G. Lozano, A. R. González-Elipe, D. Grosso, C. Boissière, C. Sanchez, G. J. A. A. Soler-Illia and H. Miguez, *J. Phys. Chem. C*, 2008, **112**, 3157–3163.

68 E. P. Degarmo, J. T. Black, R. A. Kohser and B. E. Klamecki, *Materials and Process in Manufacturing*, Wiley, 9th edn, 2003.

69 C. A. Schneider, W. S. Rasband and K. W. Eliceiri, *Nat. Methods*, 2012, **9**, 671–675.

70 J. S. Bernardes, C. A. Rezende and F. Galembeck, *Langmuir*, 2010, **26**, 7824–7832.

71 M. Faustini, M. Faustini, B. Louis, P. A. Albouy, M. Kuemmel and D. Grosso, *J. Phys. Chem. C*, 2010, **114**, 7637–7645.

72 L. Landau and B. Levich, *Acta Physicochim. URSS*, 1942, **17**, 42–54.

73 B. J. Carroll and J. Lucassen, *Chem. Eng. Sci.*, 1973, **28**, 23–30.

74 K. Kajihara and T. Yao, *J. Sol-Gel Sci. Technol.*, 2000, **17**, 173–184.

75 J. S. Bernardes, C. A. Rezende and F. Galembeck, *J. Phys. Chem. C*, 2010, **114**, 19016–19023.

76 R. P. Rand, N. Fuller, V. a. Parsegian and D. C. Rau, *Biochemistry*, 1988, **27**,, 7711–7722.

77 R. P. Rand, N. L. Fuller, S. M. Gruner and V. A. Parsegian, *Biochemistry*, 1990, **29**, 76–87.

78 A. V. Rao, A. B. Gurav, S. S. Latthe, R. S. Vhatkar, H. Imai, C. Kappenstein, P. B. Wagh and S. C. Gupta, *J. Colloid Interface Sci.*, 2010, **352**, 30–35.

79 R. Meyer, C. Lemire, S. Shaikhutdinov and H.-J. Freund, *Gold Bull.*, 2004, **37**, 72–124.

80 J. L. Gong and C. B. Mullins, *Acc. Chem. Res.*, 2009, **42**, 1063–1073.

81 F. Araiedh, F. Ducos, A. Houas and N. Chaoui, *Appl. Catal., B*, 2016, **187**, 350–356.

82 A. Zaleska, J. Nalaskowski, J. Hupka and J. D. Miller, *Appl. Catal., B*, 2009, **88**, 407–412.

83 L. Li, Y. Feng, Y. Liu, B. Wei, J. Guo, W. Jiao, Z. Zhang and Q. Zhang, *Appl. Surf. Sci.*, 2016, **363**, 627–635.

84 Y. Yuan, in *Surface Science Techniques*, ed. G. Bracco and B. Holst, Springer-Verlag Berlin Heidelberg, 2013, pp. 3–34.

85 N. Geddes, E. Paschinger and D. Furlong, *Thin Solid Films*, 1995, **260**, 192–199.

86 P. S. Foran, C. Boxall and K. R. Denison, *Langmuir*, 2012, **28**, 17647–17655.

87 C. J. van Oss, R. J. Good and R. J. Busscher, *J. Dispersion Sci. Technol.*, 1990, **11**, 75–81.

88 M. L. González-Martín, B. Janczuk, L. Labajos-Broncano, J. M. Bruque and C. M. González-García, *J. Colloid Interface Sci.*, 2001, **240**, 467–472.

89 M. Gindl, M. Gindl, G. Sinn, G. Sinn, W. Gindl, W. Gindl, A. Reiterer, A. Reiterer, S. Tschegg and S. Tschegg, *Colloids Surf., A*, 2001, **181**, 279–287.

90 C. J. Van Oss, *Interfacial Forces in Aqueous Media, Second Edition*, CRC Press, 2006.

91 S. D. Knorr, E. C. Combe, L. F. Wolff and J. S. Hodges, *Dent. Mater.*, 2005, **21**, 272–277.

92 D. V. Kilpadi and J. E. Lemons, *J. Biomed. Mater. Res.*, 1994, **28**, 1419–1425.

93 E. Chibowski and L. Holysz, *Langmuir*, 1992, **8**, 710–716.

94 Z. Kessaissia, E. Papirer and J. B. Donnet, *J. Colloid Interface Sci.*, 1981, **82**, 526–533.

95 Y. Yan, E. Chibowski and A. Szcześ, *Mater. Sci. Eng., C*, 2017, **70**, 207–215.

96 M. Kosmulski, *J. Colloid Interface Sci.*, 2014, **426**, 209–212.

97 F. Borghi, V. Vyas, A. Podestà and P. Milani, *PLoS One*, 2013, **8**, 1–14.

98 S. C. Thickett, A. Harris and C. Neto, *Langmuir*, 2010, **26**, 15989–15999.

99 S. C. Thickett, C. Neto and A. T. Harris, *Adv. Mater.*, 2011, **23**, 3718–3722.
100 S. H. Lee, P. J. Yoo, S. J. Kwon and H. H. Lee, *J. Chem. Phys.*, 2004, **121**, 4346–4351.
101 R. Seemann, S. Herminghaus, C. Neto, S. Schlagowski, D. Podzimek, R. Konrad, H. Mantz and K. Jacobs, *J. Phys.: Condens. Matter*, 2005, **17**, S267–S290.
102 R. Xie, A. Karim, J. Douglas, C. Han and R. Weiss, *Phys. Rev. Lett.*, 1998, **81**, 1251–1254.
103 J. Y. Cheng, C. A. Ross, H. I. Smith and E. L. Thomas, *Adv. Mater.*, 2006, **18**, 2505–2521.
104 J. B. Clark, J. W. Hastie, L. H. Kihlborg, R. Mtselaar and M. Thackeray, *Pure Appl. Chem.*, 1994, **66**, 577–594.
105 I. Wong, G. H. Teo, C. Neto and S. C. Thickett, *ACS Appl. Mater. Interfaces*, 2015, **7**, 21569–21570.
106 D. Fell, M. A. Dadfar, C. Liu, M. Sokuler, E. Bonaccurso and G. K. Auernhammer, *Langmuir*, 2011, **27**, 2112–2117.
107 G. Reiter and R. Khanna, *Langmuir*, 2000, **16**, 6351–6357.
108 M. W. Matsen and J. M. Gardiner, *J. Chem. Phys.*, 2001, **115**, 2794–2804.
109 L. Xue and Y. Han, *Langmuir*, 2009, **25**, 5135–5140.
110 P. Kassal, R. Šurina, D. Vrsaljko and I. M. Steinberg, *J. Sol-Gel Sci. Technol.*, 2014, **69**, 586–595.
111 Y. Lin, E. J. Petersson, Z. Fakhraai and L. I. N. E. T. Al, *ACS Nano*, 2014, **8**, 10178–10186.